Journal of Petroleum Science and Engineering 162 (2018) 446–459

Contents lists available at ScienceDirect

Journal of Petroleum Science and Engineering

journal homepage: www.elsevier.com/locate/petrol

Harmonic pulse testing for well performance monitoring

Peter A. Fokker [a,b], Eloisa Salina Borello [a,*], Francesca Verga [a], Dario Viberti [a]

[a] Politecnico di Torino, Department of Environment, Land and Infrastructure Engineering, Italy
[b] TNO/Geological Survey of the Netherlands, Utrecht, The Netherlands

ARTICLE INFO

Keywords:
Well testing
Harmonic testing
Well performance monitoring
Horizontal well
Gas storage

ABSTRACT

Harmonic testing was developed as a form of well testing that can be applied during ongoing production or injection operations, as a pulsed signal is superimposed on the background pressure trend. Thus no interruption of well and reservoir production is needed before and during the test.

If the pulsed pressure and rate signal analysis is performed in the frequency domain, strong similarity exists between the derivative of the harmonic response function versus the harmonic period and the pressure derivative versus time, typical of conventional well testing. Thus the interpretation of harmonic well tests becomes very straightforward.

In this paper, we present the analytical models for the most commonly encountered well and reservoir scenarios and we validate the model for horizontal wells against real data of a harmonic test performed on a gas storage well in Italy.

1. Introduction

For decades, well tests have been widely used by the oil industry for evaluation of well productivity and reservoir properties, which provide key information for field development and facilities design (Horne, 1994; Bourdet, 2002; Lee et al., 2003; Kamal, 2009). Recent work has been directed towards complementing conventional well tests with less expensive and/or more environmentally friendly procedures (Hollaender et al., 2002a; Holleander et al. 2002b; Beretta et al., 2007; Verga et al., 2008; Gringarten, 2008; Bertolini et al., 2009; Verga and Rocca, 2010; Verga et al., 2011, 2012, 2015; Rocca and Viberti, 2013; Verga and Salina Borello, 2016). Harmonic well testing is one of those complementing methodologies: it may not replace conventional well testing, but it can be very effective for monitoring purposes. In conventional well tests, equilibrium conditions are required in the reservoir before the test; a single well can be produced at a time, inducing one or more pressure drawdown periods followed by a final pressure build-up which are the object of the interpretation. Conversely, a harmonic test is characterized by a periodic sequence of alternating production rates which can be superimposed on the background pressure trend and thus the test can be carried out during ongoing production or injection operations.

Even if harmonic tests resemble pulse tests (Johnson et al., 1966) because of the sequence of alternating production rates, some major differences exist. Pulse tests aim at assessing hydraulic connectivity between two wells without interrupting production from other wells. In addition to pulse test purposes, harmonic tests aim at assessing well and reservoir properties, such as skin and permeability. To this end, harmonic testing analysis is performed in the frequency domain as opposed to pulse test interpretation, which relies on the pressure and pressure derivative data as in conventional well testing.

The concept of harmonic testing was first proposed by Kuo (1972) and later developed by other authors (Black and Kipp, 1981; Kazi-Aoual et al., 1991; Rosa and Horne, 1997; Hollaender et al., 2002b; Copty and Findikakis, 2004; Despax et al., 2004; Renner and Messar, 2006; Rochon et al., 2008; Ahn and Horne, 2010; Fokker and Verga, 2011; Fokker et al., 2012, 2013; Morozov, 2013; Vinci et al., 2015; Sun et al., 2015; Salina Borello et al., 2017). The main advantage of this testing approach is it does not require the interruption of production nor the knowledge of previous rate history (Hollaender et al., 2002b). In fact, the analysis in the frequency domain allows extraction and analysis of each periodic component of the pressure response in relation to the corresponding periodic component of the rate. The main drawback of harmonic testing is it takes longer to obtain the same information of conventional testing (Hollaender et al., 2002b). For this very reason, harmonic testing is inadequate for exploration and appraisal wells, but it is a valid alternative to conventional well testing for monitoring well performance.

* Corresponding author. Politecnico di Torino, Department of Environment, Land and Infrastructure Engineering, 24, Corso Duca Degli Abruzzi, 10129 Torino, Italy.
E-mail address: eloisa.salinaborello@polito.it (E. Salina Borello).
URL: http://www.polito.it/petroleum

https://doi.org/10.1016/j.petrol.2017.12.053
Received 1 August 2017; Received in revised form 26 October 2017; Accepted 16 December 2017
Available online 20 December 2017

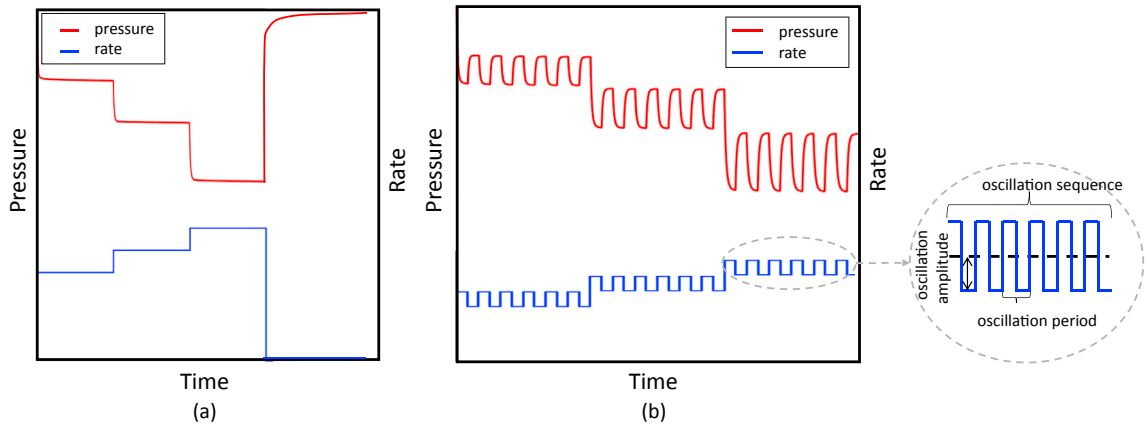

Fig. 1. Schematic of (a) a conventional well test sequence with multiple draw-downs and a build-up, compared to (b) harmonic test.

A qualitative example of conventional well test sequence (with multiple draw-downs and a build-up) compared to a harmonic test is provided in Fig. 1.

The basic concepts of harmonic testing are:

1. If a harmonic rate of given frequency is imposed to a well, the corresponding reservoir pressure response is still harmonic with the same frequency (Kuo, 1972).
2. A square pulse rate is equivalent to a linear superposition of simultaneous harmonic tests each characterized by its own frequency (Fokker and Verga, 2011).
3. The area investigated by harmonic testing is a function of the adopted rate frequencies, which should be selected in order to meet the specific testing targets (Ahn and Horne, 2010).
4. In order to maximize the information provided by harmonic pulse test (HPT) interpretation, pressure data should be adequately pre-processed adopting detrending methodologies (Ahn and Horne, 2010; Viberti, 2016) with the aim of separating pure periodic components of the signal from non-periodic components. Therefore, detrending removes aperiodicity due to temporary test interruption (i.e. well shut-in or significant rate deviation from that of the test design), generated by technical and/or operational issues.
5. Periodicity of rate variation is a basic requirement for harmonic test interpretability. However, the constant rate constraint over each flow period, strictly necessary for a conventional draw-down analysis, is relaxed in harmonic interpretation because rate fluctuations mainly affect the high frequency components (Hollaender et al., 2002b), which are relevant to the near wellbore region.
6. The log-log plot of the absolute value of the amplitude ratio between imposed rate and registered well pressure, and the amplitude ratio derivative, vs. oscillation period ($T = 2\pi/\omega$) is very similar to the conventional log-log diagnostic plot (Hollaender et al., 2002b).
7. Harmonic test response shows a phase shift, which is the relative delay of the pressure cycle with respect to the imposed flow cycle for each frequency. The phase shift can be used to assess the skin (Kuo, 1972) or to identify flow regimes (Hollaender et al., 2002b) since the plot of phase shift vs. oscillation period tends to asymptotic values for specific flow regimes. However, compared to the log-log plot, it does not provide significant additional information (Hollaender et al., 2002b).

2. Harmonic pulse testing type-curves

Harmonic test type curves can be analytically derived for different well and reservoir scenarios by solving the diffusivity equation under the condition of a harmonic rate. Because of the harmonic nature of the imposed rate and induced pressure changes, HPT interpretation involves frequency analysis. Mathematical derivations as well as synthetic validations are reported in the appendix for the reader's convenience.

The log-log plot of the absolute value of the amplitude ratio between imposed rate and registered well pressure and the amplitude ratio derivative vs. the oscillation period ($T = 2\pi/\omega$) provides diagnostic curves which are analogous to the conventional log-log diagnostic type-curves. However, despite the similarity in shape, the conventional time-domain curves are no longer applicable. In fact, a time shift of the derivative characteristic features is observed and differences exist as well between the transition periods from one flow regime to the following.

2.1. Infinite acting radial flow (I.A.R.F.)

The dimensionless solution of the diffusivity equation for an infinite-acting homogeneous and isotropic gas reservoir drained by a fully penetrating vertical well, under radial symmetry, was already published by the authors (Salina Borello et al., 2017) in terms of Hankel functions. In the present paper the dimensionless solution is given in terms of modified Bessel functions K_0 and K_1 in a form analogous to Kazi-Aoual et al., 1991:

$$m_D(T_D) = \frac{-K_0(\sqrt{i/T_D}) - S\sqrt{i/T_D}K_1(\sqrt{i/T_D})}{(1 + iSC_D/T_D)\sqrt{i/T_D}K_1(\sqrt{i/T_D}) + iC_D/T_DK_0(\sqrt{i/T_D})} \quad (1)$$

where K_0 and K_1 are the Bessel function and m_D is the dimensionless pseudo-pressure:

$$m_D = \frac{R}{\Lambda} = \frac{1}{\Lambda}\frac{m(p)_{pulser}}{q_{sc}} \quad (2)$$

R is the dimensional amplitude ratio, Λ is a factor to make the pressure over gas rate ratio dimensionless (non-dimensionalization factor):

$$\Lambda = \frac{1}{\pi kh}\frac{T_R p_{sc}}{Z_{sc}T_{sc}} \quad (3)$$

C_D is the dimensionless wellbore storage:

$$C_D = \frac{C}{2\pi\phi c_{ti}hr_w^2} \quad (4)$$

T_D is the dimensionless oscillation period:

$$T_D = \frac{1}{2\pi}\frac{kT}{\mu_i c_{ti}\phi r_w^2} \quad (5)$$

Furthermore, T is the oscillation period; k is the reservoir permeability; h is the pay thickness; ϕ is the porosity; T_R is the reservoir temperature; μ_i and c_{ti} are the gas viscosity and the total compressibility at initial conditions, respectively; Z_{sc} is the gas compressibility factor at standard conditions, which can be approximated to unity; P_{sc} and T_{sc} are

pressure and temperature at standard conditions, respectively; and S, C and r_w are the skin, wellbore storage and well radius, respectively.

Note that the argument of the Bessel function K_0 contains complex numbers; it was calculated using the algorithm by Amos (1986). In turn, also m_D assumes complex values.

It should be pointed out that equation (1) still holds true when skin incorporates non-Darcy effects (i.e. $S = \tilde{S} + Dq$), where $\tilde{S}$ is the mechanical skin, the D factor can be estimated if different HPT are conducted at different background rates.

Note that the dimensionless expressions of m_D (eq. (2)) and C_D (eq. (4)) are analogous to the ones of conventional well testing (Al-Hussainy et al., 1966; Bourdet, 2002), while T_D (eq. (5)) differs by a factor $1/2\pi$ from the conventional t_D (Al-Hussainy et al., 1966):

$$t_D = \frac{kt}{\mu_i c_{ti} \phi r_w^2} = \frac{t}{t_c} \tag{6}$$

The derivative of R vs. the oscillation period T can then be calculated by (Hollaender et al., 2002b):

$$R'(\mathrm{T}) = \frac{dR(\mathrm{T})}{dln\, T} = T\frac{dR(\mathrm{T})}{d\, T} \tag{7}$$

Being $\mathrm{R} \in \mathbb{C}$, R' assumes complex values in turn.

For very long periods, the term $1/T_D$ becomes very small. Calculating the limit of eq. (1) for $T \to \infty$ and multiplying by factor Λ (eq. (3)), the amplitude ratio and its derivative become, respectively:

$$R_{long\ T}(T) = -\frac{K_0\left(\sqrt{i/T_D}\right)}{\sqrt{i/T_D}K_1\left(\sqrt{i/T_D}\right)}\Lambda \tag{8}$$

$$T\frac{dR_{long\ T}}{dT} = -\frac{\Lambda}{2} \tag{9}$$

Eq. (9) indicates that the absolute value of the derivative tends to horizontal stabilization inversely proportional to kh. Moreover, the phase delay of eq. (8) assumes the characteristic value $\angle R = \angle\text{-}1 = \pi$.

It is easy to verify that for $T \to \infty$:

$$T\left|\frac{dR_{long\ T}}{dT}\right| = T\frac{d\left|R_{long\ T}\right|}{dT} \tag{10}$$

At short times, C_D/T_D becomes very large and wellbore storage dominates. Calculating the limit of eq. (1) for $T \to 0$ and multiplying by factor Λ, the response function and the derivative become, respectively:

$$R_{short\ T} = i\frac{T_D}{C_D}\Lambda \tag{11}$$

$$T\frac{dR_{short\ T}}{dT} = i\frac{T_D}{C_D}\Lambda = R_{short\ T} \tag{12}$$

Thus, the modulus of the response and the modulus of the response derivative both follow a linear trend with T, which corresponds to a line with a unit slope on a log-log plot. In this case the phase delay assumes the characteristic value $\angle R = \angle\, i = \pi/2$.

Analogously to conventional well test analysis, the modulus of the amplitude ratio (|R|) and the modulus of its derivative with respect to lnT (|R'|) are plotted against the corresponding oscillation period (T) on a log-log scale and the match point (x_M, y_M) is selected at the intercept of the horizontal stabilization and the linear wellbore storage trend. Thus for the gas reservoir we have:

$$kh = \frac{1}{4\pi}\frac{2T_R p_{sc}}{Z_{sc}T_{sc}}\frac{1}{y_M} \tag{13}$$

$$C = 2x_M\frac{kh}{\mu} \tag{14}$$

It should be pointed out that, except for very early times and for late time behavior, the derivative of the modulus of R $\left(|R|' = T\frac{d|R|}{dT}\right)$ and the modulus of the derivative of R $\left(|R'| = T\left|\frac{dR}{dT}\right|\right)$ are not equal. A typical plot for R and R' is presented in Fig. 2 where both the derivatives of the modulus of R (|R|') and the modulus of the derivative of R (|R'|) are given. Note that wellbore storage effects last longer on |R'|.

A comparison of the proposed model in the frequency domain with a standard well test log-log plot for a single flow period is possible when proper non-dimensionalizations are adopted:

- *dimensionless log-log plot in the frequency domain*: the modulus of the dimensionless pseudopressure in the frequency domain m_D (|R/Λ|), calculated according to eq. (1), and the modulus of its derivative with respect to lnT (|R'/Λ|) are plotted against the dimensionless oscillation period (T_D), calculated according to eq. (5);
- *dimensionless log-log plot in the time domain*: the dimensionless pseudopressure changes in the time domain (Δm(p)/Λq) and its derivative with respect to ln t (Δm'(p)/Λq) are plotted against the dimensionless time t_D (eq. (6)).

The comparison is shown in Fig. 3. Notice that time derivatives are concordant in dimensionless time, which means that a lag factor 2π exists between oscillation period vs. elapsed time if the same investigation distance is considered (see eq. (5) vs. eq. (6)).

2.2. Horizontal well

Fluid flow in a reservoir drained by a horizontal well cannot be described by a 2D equation in the near wellbore zone. An alternative approach is required, and we have developed a similar approach to that described by Fokker and Verga (2008). Thus, we first split the well into segments of equal lengths (L_{seg}). The overall pressure response is given by the superposition of the responses due to each producing well segment (j). The fluxes into the segments are finally determined by requiring a prescribed total flux and a constant pressure over the well.

The solution of diffusivity equation at the well with a pulsing rate of period T_D reads (see Appendix A.1 for details):

$$m_D(T_D) = \frac{1}{\sum_{ij}\left[\Gamma^{well} - \mathrm{S}\frac{\mathrm{h}}{\mathrm{L_{seg}}}\mathrm{I}\right]^{-1}_{ij} - \mathrm{i}\frac{C_D}{\mathrm{T_D}}} \tag{15}$$

where Γ^{well} is the matrix with values of Γ_{ij} calculated for segment position

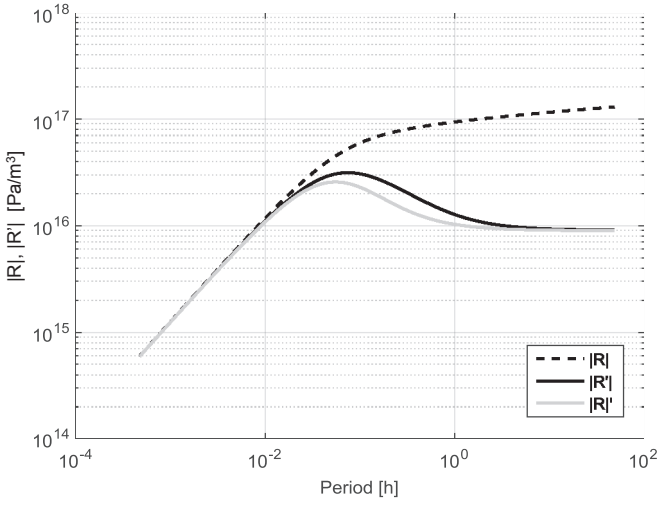

Fig. 2. I.A.R.F. model: comparison between |R|′ and |R′|.

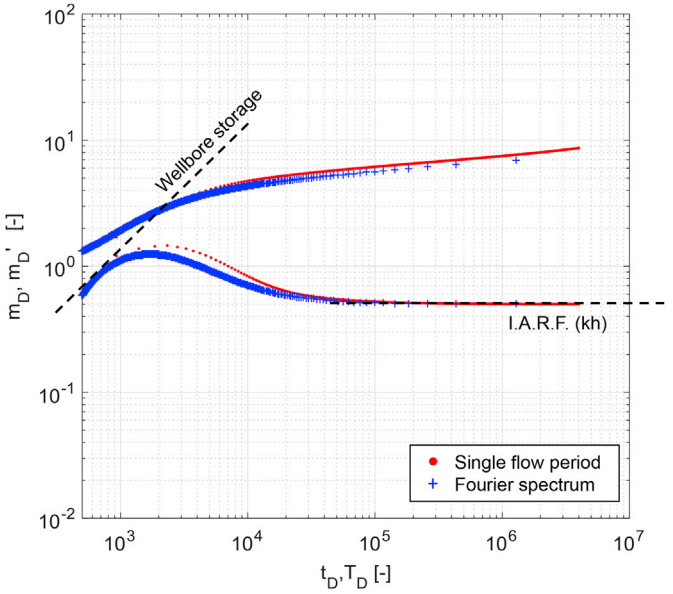

Fig. 3. Response of a fully penetrating well in an infinite-acting reservoir: comparison, in dimensionless terms, between the pressure derivative in time of a single flow period (red) and the derivative in period of the Fourier spectrum of the entire oscillation sequence (blue). (For interpretation of the references to colour in this figure legend, the reader is referred to the Web version of this article.)

i due to reservoir fluid flow into segment j (eq. (A.20)), and L_{seg} is the length of the well segment.

In the presence of vertical anisotropy, eq. (15) holds with:

$$[x, y, z]^{eq} = \left[\frac{x}{\sqrt{\alpha}}, \frac{y}{\sqrt{\alpha}}, z\sqrt{\alpha}\right] \tag{16}$$

$$h^{eq} = h\sqrt{\alpha} \tag{17}$$

$$L_{seg}^{eq} = \frac{L_{seg}}{\sqrt{\alpha}} \tag{18}$$

$$r_w^{eq} = \frac{1+\alpha}{2\sqrt{\alpha}} r_w \tag{19}$$

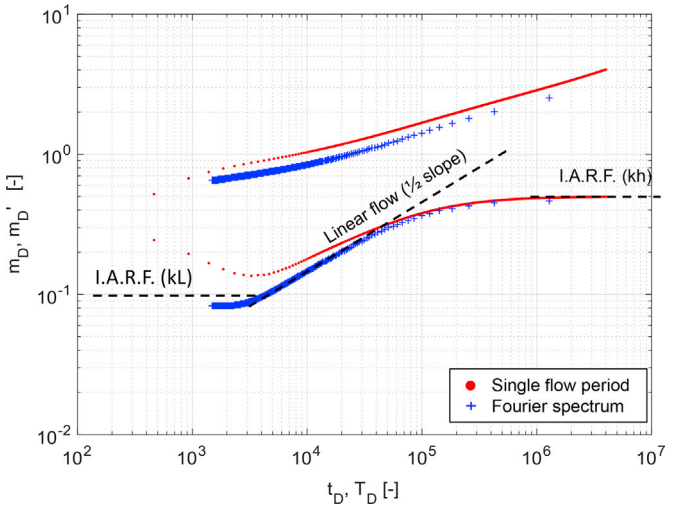

Fig. 4. Response of a fully penetrating horizontal well (L = 5h): comparison, in dimensionless terms, of the pressure derivative in time of a single flow period (red) vs. the derivative in period of the Fourier spectrum of the entire oscillation sequence (blue). (For interpretation of the references to colour in this figure legend, the reader is referred to the Web version of this article.)

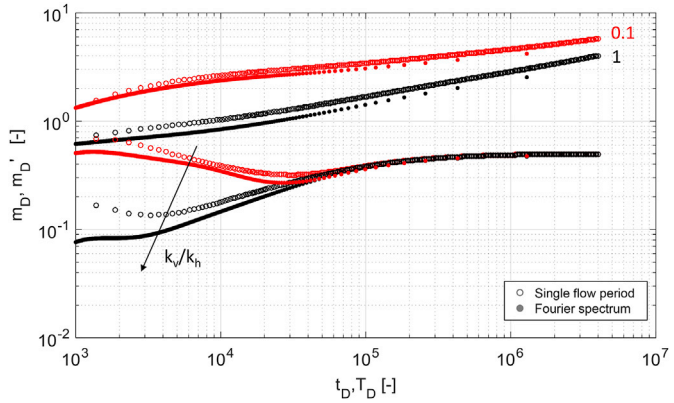

Fig. 5. Anisotropy effects ($k_v/k_h = 1$, 0.1) on the pressure derivative in time of a single flow period (empty dots) vs. the derivative in period of the Fourier spectrum of the entire oscillation sequence (full dots), in dimensionless terms, for a horizontal well with L = 5h.

$$T_D^{eq} = T_D \frac{4}{(1+\alpha)^2} \tag{20}$$

where

$$\alpha = \sqrt{\frac{k_h}{k_v}} \tag{21}$$

Details are given in appendixes A.1 and A.2.

In the horizontal well scenario a numerical approach is more convenient to calculate the derivative of R. Comparison in dimensionless terms between the |R'| and the pressure derivative in time of a single flow period is shown in Figs. 4 and 5. Log-log plots are concordant in dimensionless time (Fig. 4), even in the presence of vertical anisotropy (Fig. 5). Notice that, similarly to the pressure derivative in time, the derivative of R vs. period is initially dominated by wellbore storage; then it stabilizes at $\sqrt{k_h k_z}L$, corresponding to radial flow developing in a vertical plane orthogonal to the well axis; subsequently, linear flow develops and finally the kh stabilization is reached. Discussion and validation of this model is given in appendix A.3.

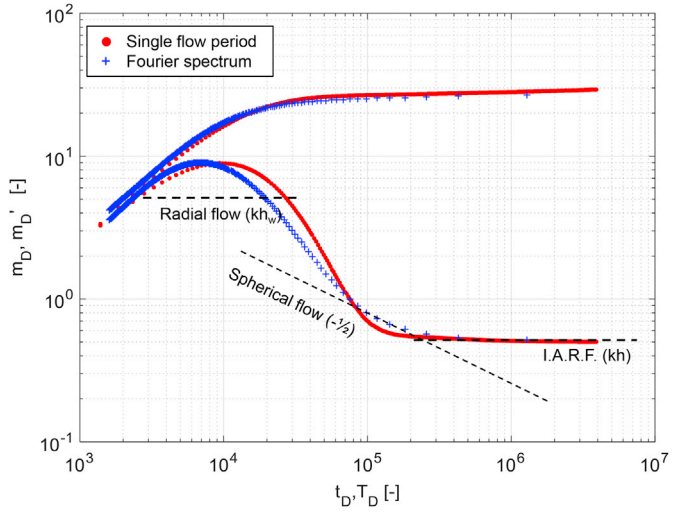

Fig. 6. Response of a partially penetrating vertical well ($h_w/h = 0.1$): comparison, in dimensionless terms, between the pressure derivative in time of a single flow period (red) and the derivative in period of the Fourier spectrum of the entire oscillation sequence (blue). (For interpretation of the references to colour in this figure legend, the reader is referred to the Web version of this article.)

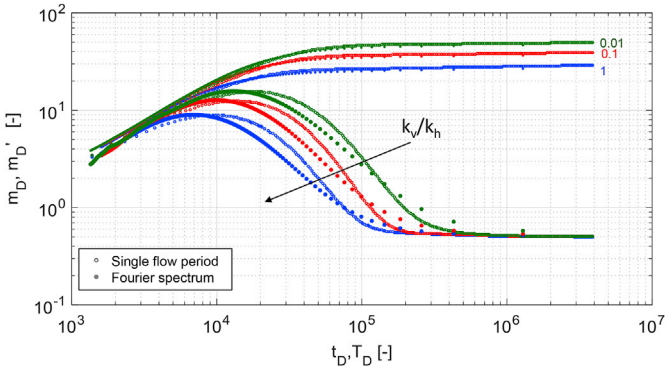

Fig. 7. Anisotropy effect (k_v/k_h =1, 0.1, 0.01) on the pressure derivative in time of a single flow period (empty dots) vs. the derivative in period of the Fourier spectrum of the entire oscillation sequence (full dots), in dimensionless terms, for a partially penetrating vertical well ($h_w/h = 0.1$).

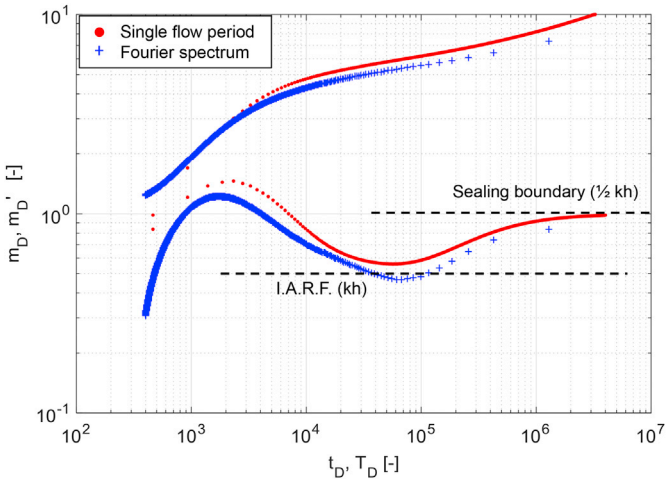

Fig. 8. Response of a pulser well in a single boundary scenario ($d_F = 500\ r_w$): comparison, in dimensionless terms, of the pressure derivative in time of a single flow period (red) vs. the derivative in period of the Fourier spectrum of the entire oscillation sequence (blue). (For interpretation of the references to colour in this figure legend, the reader is referred to the Web version of this article.)

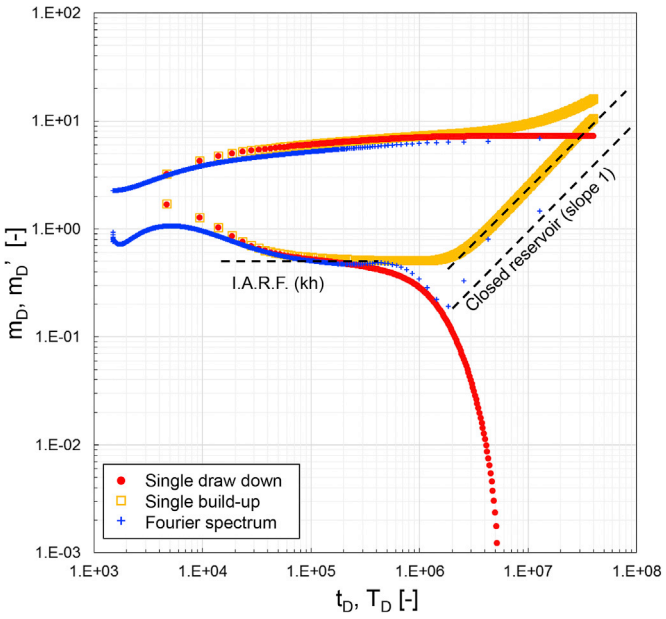

Fig. 9. Response of a pulser well in a closed reservoir scenario ($r_e = 3000\ r_w$): comparison, in dimensionless terms, of the pressure derivative in time of a single flow period (build-up in red dots, draw-down in yellow squares) vs. the derivative in period of the Fourier spectrum of the entire oscillation sequence (blue crosses). (For interpretation of the references to colour in this figure legend, the reader is referred to the Web version of this article.)

2.3. Partial penetration model

The type-curves of a limited entry well can be developed in a way very similar to that of a horizontal well (see appendix A.1 and A.2). The main difference is the flux orientation with respect to the Cartesian axes.

Comparison in dimensionless terms between the $|R'|$ and the pressure derivative in time of a single flow period is shown in Figs. 6 and 7. The log-log plot shows that the derivatives are quite concordant in dimensionless time (Fig. 6), even in the presence of vertical anisotropy (Fig. 7).

2.4. One fault model

If a single no-flow boundary exists at distance d_F from the well, the contribution of an image well at distance $2d_F$ from the well is added to the I.A.R.F. model (eq. (1)), giving:

$$m_D(T_D) = \frac{-K_0(\sqrt{i/T_D}) - S\sqrt{i/T_D}K_1(\sqrt{i/T_D}) - K_0\left(\frac{2d_F}{r_w}\sqrt{i/T_D}\right)}{(1+iSC_D/T_D)\sqrt{i/T_D}K_1(\sqrt{i/T_D}) + iC_D/T_D K_0(\sqrt{i/T_D})} \tag{22}$$

Comparison in dimensionless terms between $|R'|$ and the pressure derivative in time of a single flow period is shown in Fig. 8. Again, the log-log plots are quite concordant in dimensionless time.

2.5. Closed boundary

The solution for a closed gas reservoir is found by imposing no-flow boundary conditions at distance r_e, giving:

$$m_D(T_D) = \frac{-\left[K_0\left(\sqrt{i/T_D}\right)I_1\left(\frac{r_e}{r_w}\sqrt{i/T_D}\right) + K_1\left(\frac{r_e}{r_w}\sqrt{i/T_D}\right)I_0\left(\sqrt{i/T_D}\right)\right] - S\sqrt{i/T_D}\left[K_1\left(\sqrt{i/T_D}\right)I_1\left(\frac{r_e}{r_w}\sqrt{i/T_D}\right) + K_1\left(\frac{r_e}{r_w}\sqrt{i/T_D}\right)I_1\left(\sqrt{i/T_D}\right)\right]}{(1+iSC_D/T_D)\sqrt{i/T_D}\left[K_1\left(\sqrt{i/T_D}\right)I_1\left(\frac{r_e}{r_w}\sqrt{i/T_D}\right) - K_1\left(\frac{r_e}{r_w}\sqrt{i/T_D}\right)I_1\left(\sqrt{i/T_D}\right)\right] + iC_D/T_D\left[K_0\left(\sqrt{i/T_D}\right)I_1\left(\frac{r_e}{r_w}\sqrt{i/T_D}\right) + K_1\left(\frac{r_e}{r_w}\sqrt{i/T_D}\right)I_0\left(\sqrt{i/T_D}\right)\right]} \tag{23}$$

As shown in Fig. 9, when the investigation distance r_e is reached, the derivative of Fourier spectrum firstly decreases with a trend similar to that of the build-up derivative; successively for $T_D \to \infty$ it rises with slope 1, analogously to draw-down derivative.

3. Application to a real case

The proposed methodology was applied to a real gas storage well. The areal dimension of the reservoir is 3.4 × 1.1 km^2. Reservoir pressure and temperature at test time were 90 bar and 44.7 °C, respectively. The porosity in the pulser area is 0.14, the total compressibility is 0.0111405 bar^{-1}. The gas is 94.5% methane, 3.5% ethane, 1% propane, 1% nitrogen. The well (well diameter $r_w = 9^{5/8}$ inches) is horizontal with a producing horizontal length of 161.6 m, navigating in the first 9 m of

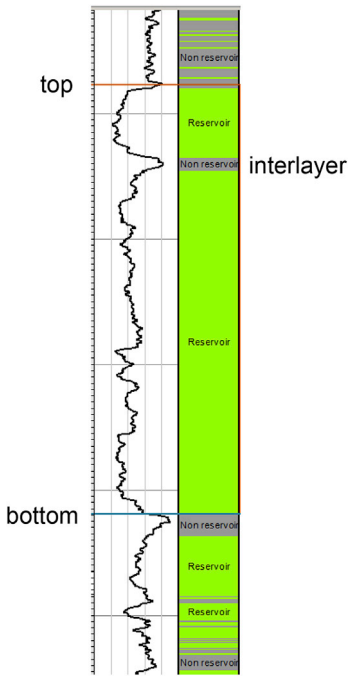

Fig. 10. Pilot well Gamma-ray log.

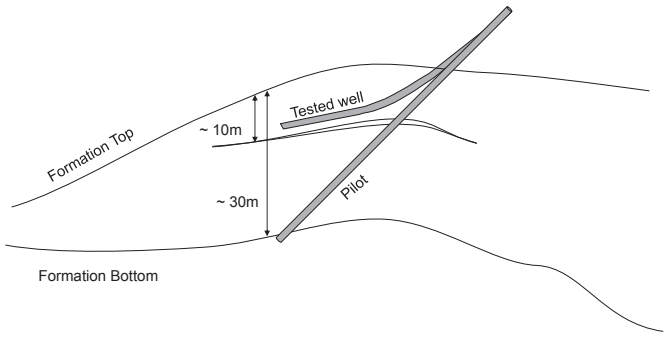

Fig. 11. Sketch of the reservoir cross-section.

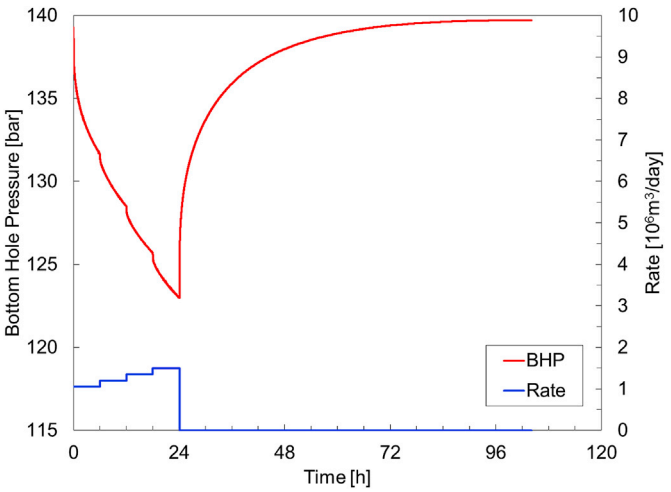

Fig. 13. Rate history (blue) and registered BHP (red) of the FAF test Dec. 2014. (For interpretation of the references to colour in this figure legend, the reader is referred to the Web version of this article.)

Table 1
List of available well test for comparison.

Date	Test type	Notes	Interpretation
Dec. 2014	FAF	Preliminary shut-in Nearby wells shut during the test	Conventional
Mar. 2016	HPT	Storage under production. No well closure	Harmonic

the reservoir pay.

The tested well departs from a slanted pilot well which crosses the entire net pay; a gamma ray log run in the pilot (Fig. 10) shows the presence of a clay interlayer at 10 mTVD from the top. Therefore, a net pay of 10 m was adopted in the interpretation. A sketch of the reservoir cross-section is shown in Fig. 11.

A square pulsing test with constant productions of $\pm 50\,10^3$ Sm^3/day, lasting 24 h each, was superposed on a background field production of $450\,10^3$ Sm^3/day. Pressures were recorded downhole every 10 s (resolution = 0.0007 bar, accuracy = ±0.02% full scale), while rates were

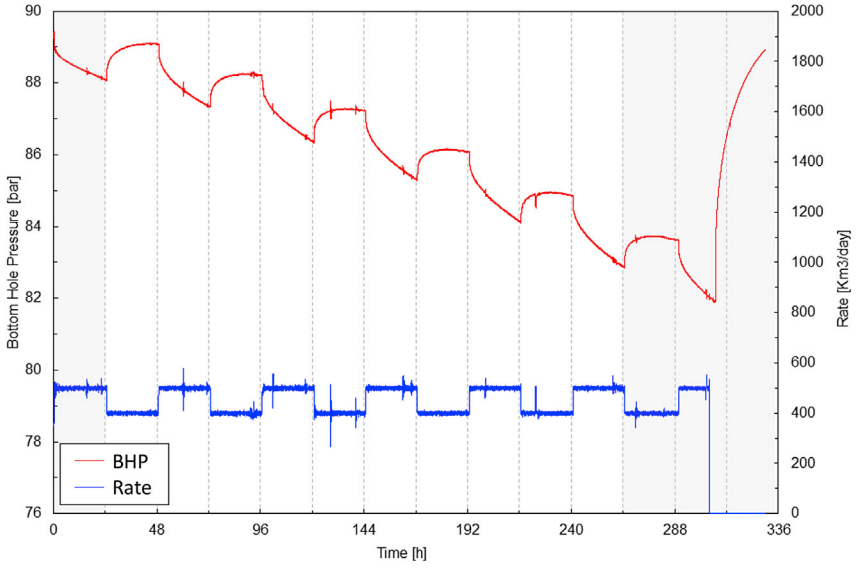

Fig. 12. Rate history (blue) and registered BHP (red) of the HPT test Mar. 2016. The first and the last two hemi-periods were discarded to maximize data regularity. (For interpretation of the references to colour in this figure legend, the reader is referred to the Web version of this article.)

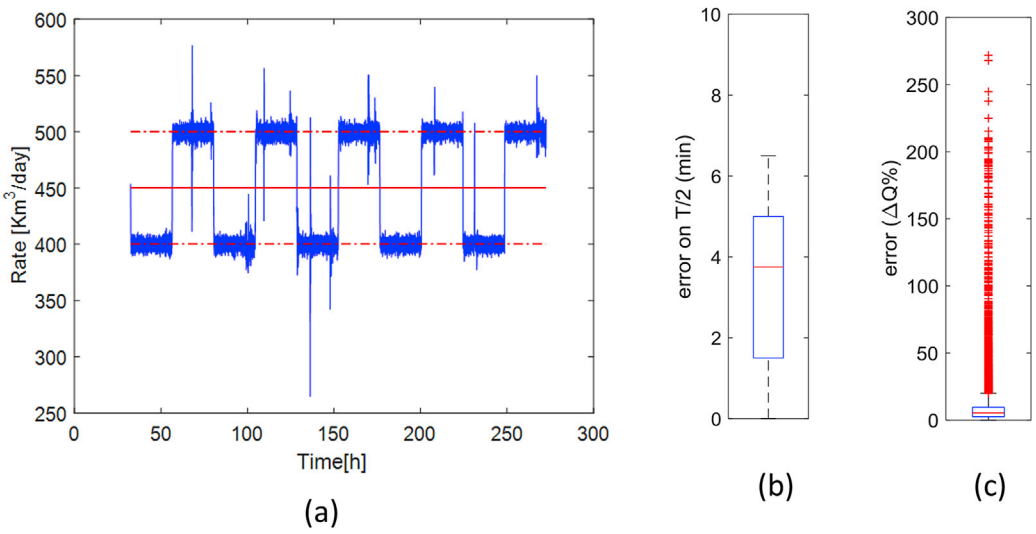

Fig. 14. Rate data quality check.

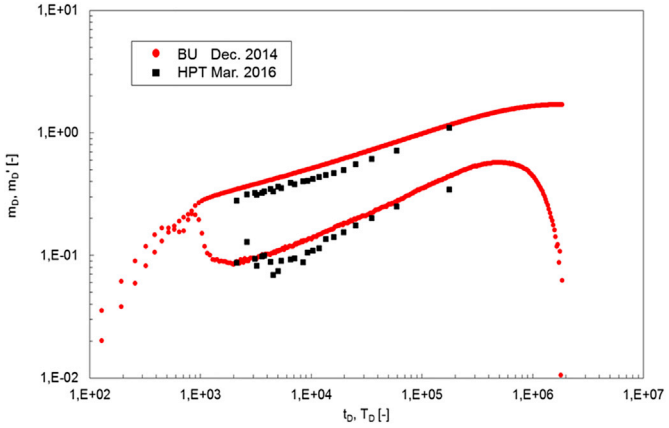

Fig. 15. Comparison of dimensionless derivatives from HPT and FAF test.

recorded at the well head every 30 s. Production rates and pressures recorded during the two tests are reported in Fig. 12. A preexisting Flow After Flow (FAF) test was also available for the same well (see Fig. 13 and Table 1). The results from the interpretation of the FAF test, which involved higher rates with respect to those produced during the HPT, clearly showed negligible non-Darcy effects. This result is in agreement with the expected skin component due to non-Darcy effect calculated for the HPT test (see appendix A.4 for details).

Table 2
Comparison of interpretation results obtained from different tests and/or with different approaches.

	FAF BU Dec. 2014	HPT Mar. 2016
k (mD)	34	39
S (-)	0.2	0
C (Pa/m^3)	2 10^{-5}	2 10^{-5}

3.1. Results and discussion

Preliminarily, a rate resampling was performed following a step-wise constant approach, in order to have the same sampling of bottom-hole pressure data. Subsequently, a quality check on pressure and rate data was conducted. Rate data were sufficiently regular (Fig. 14) both in time (3° quartile of error distribution on hemi-period duration below 5 min over 24 h) and value (3rd quartile of error distribution on rate change about 10%). As a consequence the signal to noise ratio was about 5. Pressure data showed a similar signal to noise ratio ($\Delta p_{osc} \sim \pm$ 0.5 bar,

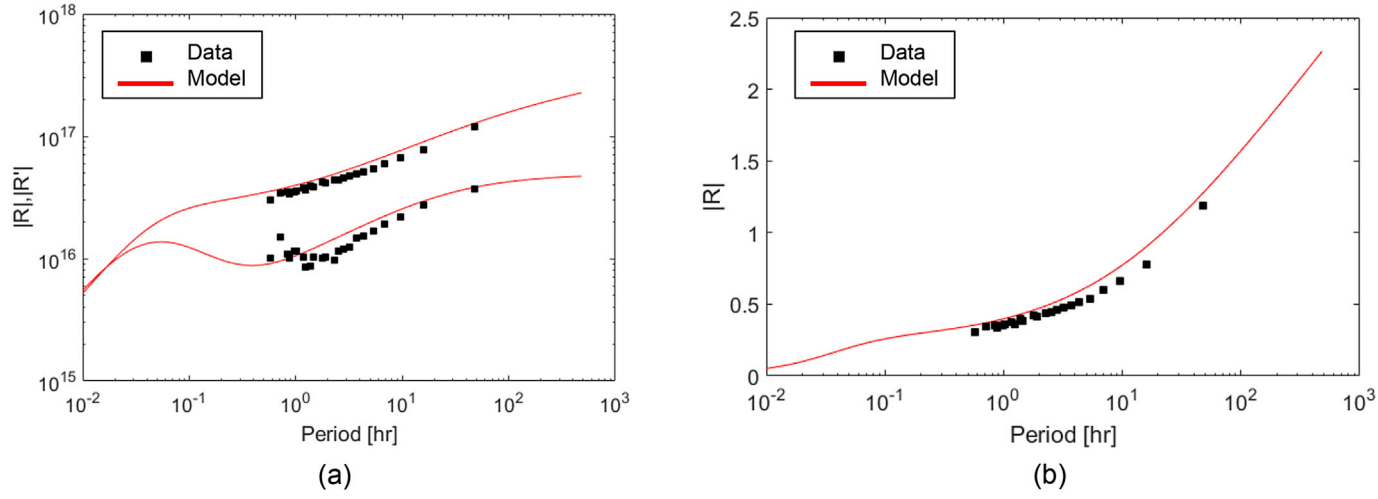

Fig. 16. Match of the HPT test data in the frequency domain: analogous of log-log plot (a) and Horner plot (b).

$\Delta p_e \sim \pm 0.1$ bar) which is ascribed to rate irregularity.

Then bottom-hole pressure data were processed in the frequency domain by applying the Fast Fourier Transform. The normalized pseudo-pressure and its derivative vs. oscillation period plotted on a log-log scale was compared, in dimensionless terms, with the conventional log-log plot of the build-up (BU) of the preexistent FAF test (Fig. 15). Derivatives were in good agreement.

Interpretation of the HPT with the type-curve of eq. (15) is shown in Fig. 16. Interpretation results in terms of well and petrophysical properties are listed in Table 2 and compared with the build-up interpretation of the preexistent FAF test. Good agreement was found.

4. Conclusions

Analytical models for HPT interpretation on a graph analogous to the log-log diagnostic plot, but applied to the frequency domain, were derived and synthetically validated for the most common scenarios (I.A.R.F., single boundary, partial penetration, horizontal well, closed reservoir).

By defining a non-dimentionalization factor for oscillation period equal to $2\pi\, t_c$, good correspondence with the conventional log-log plot in dimensionless terms was observed for all models with the only exception of the transition zones. This implies that:

1. An interpretation approach analogous to conventional well test can be adopted – provided that adequate data processing and specific analytical solutions are implemented.
2. A 2π lag factor exists between the investigation distance from a conventional test with build-up duration t and a harmonic pulse test with oscillation period $T = t$.

This, in addition to a minimum number of 5 oscillation periods needed for HPT to be robust, confirms that HPT takes much longer than conventional well testing to obtain the same information. Thus, the longer duration needed for HPT makes it less suitable for late time investigation, such as field boundary identification. Conversely, an important value of the proposed approach, which is not meant to be a substitute for a standard test, lies in the possibility of monitoring well performance without significant field operation alterations.

The procedure for harmonic test interpretation was successfully applied to a horizontal well producing a gas storage reservoir with ongoing operations. The dimensionless log-log plot of the derivative of the amplitude ratio in the frequency domain was in good agreement with conventional build-up pressure derivative and the well test interpretation with the developed type-curves gave consistent results.

Acknowledgements

The authors would like to acknowledge Stogit S.p.A. for kindly providing the data of the case history presented in this paper.

Nomenclature

β	turbulence factor, 1/L
$\mathbf{\Gamma}$	matrix of the pressure (or pseudo-pressure) field accounting for well segments contributions, dimensionless
μ	gas viscosity, m/Lt
Λ	non-dimensionalization factor, $(m/L^4t^2)^{-1}$
ϕ	porosity, dimensionless
ω	angular frequency, θ/t
B	gas volume factor, dimensionless
C	wellbore storage, L^4t^2/m
C_D	dimensionless wellbore storage
c_t	total compressibility, Lt^2/m
D	non Darcy coefficient, $(L^3/t)^{-1}$
d_F	distance of single boundary from well, L
g_ω	pressure (or pseudo-pressure) response of the well for component ω, m/Lt^2 (m/Lt^3 for gas)
g_ω^j	pressure (or pseudo-pressure) response of the well segment j for component ω, m/Lt^2 (m/Lt^3 for gas)
$\boldsymbol{g_\omega}$	vector of the pressure (or pseudo-pressure) responses of the well segments for component ω, m/Lt^2 (m/Lt^3 for gas)
h	pay thickness, L
k	permeability, L^2
m	pseudo-pressure, m/Lt^3
m_D	dimensionless pseudo-pressure
p	pressure, m/Lt^2
$\tilde{q}_\omega^{well}$	scaled rate for the harmonic component ω including wellbore storage, m/Lt^2 (m/Lt^3 for gas)
$\tilde{q}_\omega^{sf}$	scaled rate sand-face (no wellbore storage) for the harmonic component ω, m/Lt^2 (m/Lt^3 for gas)
$\tilde{q}_\omega^{j.sf}$	scaled rate sand-face of the well segment j for component ω, m/Lt^2 (m/Lt^3 for gas)
R	amplitude ratio $m(p)/q_{sc}$, m/L^4t^2
R'	derivative of amplitude ratio vs. T, m/L^4t^2
r_e	external radius, L
r_w	well radius, L
S	skin, dimensionless
t_c	characteristic time, t
T	oscillation period, t
T_f	fundamental oscillation period, t

T_D	dimensionless oscillation period
T_D^{eq}	dimensionless oscillation period for the equivalent isotropic scenario
t_D	dimensionless time
T_R	reservoir temperature, T
Z	gas compressibility factor, dimensionless
∠R	phase delay, θ

Constants

i	imaginary unit, dimensionless
T_{sc}	*temperature at standard conditions, 293.15 K*
p_{sc}	pressure at standard conditions, 101.325 kPa
R	gas constant, 8.314472 J K^{-1} mol^{-1}

Appendix

A.1 Development of the horizontal well solution

Flow in the reservoir close to a horizontal well cannot be described by a 2D equation. We used a similar approach to that of Fokker and Verga (2008). We split the well up into segments, calculated the pressure response of each segment due to the flow into said segment and into the others, and chose the fluxes into each segment in a way that the total flow was the prescribed value and the pressures were the same for all segments. The no-flow conditions at the upper and lower reservoir boundaries were fulfilled by positioning a vertical array of image sources.

In a homogeneous and isotropic reservoir containing slightly compressible fluid, the flow is described by the diffusivity equation:

$$\phi c_t \frac{\partial p}{\partial t} = \nabla\left[\frac{k}{\mu}\nabla p\right] \tag{A.1}$$

where ϕ is the rock porosity, c_t is the total compressibility, k is the rock permeability, μ is the fluid viscosity, p is the pressure and t is the time.

In gas reservoirs, an analogous equation can be written by using the pseudo pressure function:

$$\frac{m(p) = 2\int_{p_b}^{p} \tilde{p} d\tilde{p}}{\mu Z} \tag{A.2}$$

where Z is the gas compressibility factor and the limits of integration are between a base pressure p_b and the pressure of interest p.

This pseudo pressure is a standard function of pressure which was designed to linearize the diffusivity equation for gas (see, e.g. Al-Hussainy et al., 1966). We obtained:

$$\phi c_t \frac{\partial m}{\partial t} = \nabla\left[\frac{k}{\mu}\nabla m\right] \tag{A.3}$$

When a piecemeal homogeneous subsurface is assumed, the diffusivity equation for oil is linear. For gas, it is not (the product μc_t depends on $m(p)$), but we treated the equation as linear by assuming small pressure disturbances. We obtained:

$$\frac{\partial m}{\partial t} = \eta \nabla^2 m \tag{A.4}$$

where:

$$\eta = \frac{k}{\phi \mu c_t} \tag{A.5}$$

Under the assumption of linearity, the pressure and flow solution of a reservoir with many wells and changing production rates could then be added to the solution of the harmonic test. A Fourier transformation (FFT) picked out the signal present in the imposed frequency. Furthermore, there was no frequency mixing. Therefore, we considered each frequency component independently. The final pressure was then a superposition of the responses to all the frequency components present in the imposed flow rate, added to the background signal.

We wrote the pseudo-pressure solution for each frequency as the product of a space-dependent and a time-dependent function:

$$m_\omega(\boldsymbol{r}, t) = g_\omega(\boldsymbol{r}) e^{i\omega t} \tag{A.6}$$

The angular frequency was defined as $\omega = 2\pi/T$, with T the oscillation period of the imposed harmonic signal. This resulted in a time-independent differential equation for g:

$$i\omega g_\omega(\boldsymbol{r}) = \eta \nabla^2 g_\omega(\boldsymbol{r}) \tag{A.7}$$

The case for an oil reservoir is the same, with the pressure p replacing the pseudo-pressure m.

For the scaling of the volumetric rates, we took for the two cases:

$$\tilde{q}^{gas} = \frac{2p_{sc}T_R}{Z_{sc}T_{sc}}\frac{q^{gas}}{2\pi hk} = \Lambda_{gas}q^{gas} \tag{A.8}$$

$$\tilde{q}^{oil} = B\mu\frac{q^{oil}}{2\pi hk} = \Lambda_{oil}q^{oil} \tag{A.9}$$

in which B is the formation volume factor and h is the reservoir thickness, q^{gas} and q^{oil} are rates at standard conditions; the rate is taken positive for production.

Considering a point source as a fundamental solution, the diffusivity equation for the pressure amplitude around it (eq. (A.7)) can be written as:

$$\zeta^2 g_\omega(r) = \frac{1}{r^2}\frac{d}{dr}\left(r^2\frac{dg_\omega}{dr}\right) \tag{A.10}$$

where:

$$\zeta = \sqrt{\frac{i\omega}{\eta}} = \frac{1}{r_w}\sqrt{\frac{i}{T_D}} \tag{A.11}$$

Equation (A.10) is known as a spherical Bessel equation, or alternatively, a Helmholtz equation.

For an infinite reservoir, the pressure disturbance vanishes at large distances from the well, as the net flow of the harmonic signal is zero (first boundary condition):

$$[g_\omega]_{r\to\infty} = 0 \tag{A.12}$$

The second boundary condition is a harmonic signal on the flow rate into the well, corrected for the wellbore storage effect. In first instance the source flux was calculated at the sand face and was referred to as $\tilde{q}^{sf}_\omega$, to distinguish it from the $\tilde{q}^{well}_\omega$ introduced later on, which included the wellbore storage.

The fundamental solution for a point source in infinite space with vanishing pressure disturbance far away from the source, with strength $\tilde{q}^{sf}_\omega$ read:

$$g^{p}_\omega(r) = -\frac{h}{2}\frac{\exp[-\zeta r]}{r}\tilde{q}^{sf}_\omega \tag{A.13}$$

The factor $h/2$ was introduced for convenience and as a means to make the expression non-dimensional.

In a finite-thickness horizontal layer with thickness h, the boundary conditions at the upper and lower boundaries were fulfilled by complementing this function with a 1-dimensional series of images. The expression for a point source in a horizontal layer was:

$$g^{pL}_\omega(r) = \gamma_\omega\tilde{q}^{sf}_\omega \tag{A.14}$$

where:

$$\gamma_\omega = -\frac{h}{2}\sum_k\frac{\exp[-\zeta r_k]}{r_k} \tag{A.15}$$

in which:

$$r_k = \sqrt{\rho^2 + (z - z_k)^2} \tag{A16}$$

and the index k ranges over the image sources. We used Poisson's formula to obtain a rapidly converging series of the Fourier transforms for values of $|\zeta| < 1$ (van Kruysdijk, 1988). The expression became:

$$\gamma_\omega = -\frac{h}{2}\frac{2}{h}\left\{K_0(\zeta\rho) + 2\sum_{n=1}^{\infty}K_0\left(\rho\sqrt{\zeta^2 + (n\pi/h)^2}\right)\cos\left(\frac{n\pi z}{h}\right)\cos\left(\frac{n\pi z_j}{h}\right)\right\} \tag{A.17}$$

$$\rho^2 = (x - x_j)^2 + (y - y_j)^2 \tag{A.18}$$

where (x_j, y_j, z_j) denotes the position of the jth segment along the well and K_0 is the modified Bessel Function of the second kind.

The choice of the first or the second expressions for γ_ω (eq. (A.15) or (A.17), respectively) depends on the values of ζ and the distance to the source; this way any singularities of the Bessel function are avoided and the computation times minimized.

The pressure response at any position r_i due to a producing well segment j with a homogeneous distribution of the flux is an integral of this function

over the well segment

$$g_{\omega}^{j,sf}(r_i) = \Gamma_{ij}\tilde{q}_{\omega}^{j,sf} \tag{A.19}$$

$$\Gamma_{ij} = \Gamma_j(r_i) = \int_0^1 \gamma_{\omega}\left[r_i(s_j)\right]ds_j \tag{A.20}$$

where the variable s_j denotes the relative position along the well segment: while it changes from 0 to 1 the position (x_j, y_j, z_j) changes from the beginning to the end of the segment. We employed numerical integration.

We then proceeded to employ a pressure boundary condition in the well to determine the strengths of the different well segment sources.

The pressure at any point in the reservoir is the summation of the contributions from all well segments j. Therefore, the pressure amplitude at any position r_i due to all the segments read:

$$g_{\omega}(r_i) = \sum_j \Gamma_{ij}\tilde{q}_{\omega}^{j,sf} \tag{A.21}$$

The pressure inside the well in a segment i presents a difference with the pressure in the reservoir, due to skin:

$$\Delta g_{\omega S} = S\frac{h}{L_{seg}}\tilde{q}_{\omega}^{i,sf} \tag{A.22}$$

Thus, the pressure inside the well ($r = r_w$) in a segment i is:

$$g_{\omega}(r_w) = \left(\sum_j \Gamma_{ij}\tilde{q}_{\omega}^{j,sf} - S\frac{h}{L_{seg}}\tilde{q}_{\omega}^{i,sf}\right) \tag{A.23}$$

The summation only operated on the first term, in which the influence of all well segments were modelled. The second term only operated on the flux that entered the segment under consideration. The collection of pressures in all segments i could thus be represented as a superposition of contributions of production into all segments, and a skin term dependent on the flux into that particular segment. Representing the collection of these terms into a vector we wrote in vector notation:

$$\mathbf{g}_{\omega} = \left(\mathbf{\Gamma}^{well} - S\frac{h}{L_{seg}}\mathbf{I}\right)\tilde{\mathbf{q}}_{\omega}^{sf} \tag{A.24}$$

where $\mathbf{g}_{\omega}$ is the vector of yet unknown pressure amplitudes in the well; $\mathbf{\Gamma}^{well}$ is the matrix with values of Γ_{ij} calculated for segment position i due to reservoir fluid flow into segment j. Notice that $\mathbf{\Gamma}^{well}$ is a matrix of complex numbers.

If friction in the well is negligible, the pressure is constant – its magnitude being dependent on total rate magnitude and frequency. All elements of the vector $\mathbf{g}_{\omega}$ must then be identical to a single value g_{ω}. We therefore inverted eq. (A.24) to calculate the distribution of fluxes over the segments of the well:

$$\tilde{\mathbf{q}}_{\omega}^{sf} = \left(\mathbf{\Gamma}^{well} - S\frac{h}{L_{seg}}\mathbf{I}\right)^{-1}\mathbf{g}_{\omega} \tag{A.25}$$

where $\tilde{\mathbf{q}}_{\omega}^{sf}$ is the vector of all fluxes into well segments. These fluxes do not have to be identical – an infinite-conductivity horizontal well typically shows larger influx towards the two producing endpoints.

To incorporate the wellbore storage effect, the sum of all segment fluxes must be corrected for it. We have:

$$\tilde{q}_{\omega}^{well}e^{i\omega t} = \sum_i \tilde{q}_{\omega}^{i,sf}e^{i\omega t} - \frac{1}{\eta}r_w^2 C_D\frac{\partial}{\partial t}(m_{\omega}(r_w, t)) \tag{A.26}$$

giving, after the substitution of eqs. (A.25) and (A.6) and the definition of the appropriate parameters:

$$\tilde{q}_{\omega}^{well} = \sum_i \left[\left(\mathbf{\Gamma}^{well} - S\frac{h}{L_{seg}}\mathbf{I}\right)^{-1}\mathbf{g}_{\omega}\right]_i - i\frac{1}{T_D}C_D g_{\omega} \tag{A.27}$$

The terms within the square brackets of eq. (A.27) combine to the sum of the ist row of the inverted matrix, multiplied by the constant number g_{ω}. The result of the complete summation is therefore the summation of all elements of the inverse matrix multiplied by the constant number g_{ω}. The response function was then given by:

$$m_D(\mathrm{T}_D) = \frac{m_{\omega}(r_w,\ t)}{\tilde{q}_{\omega}e^{i\omega t}} = \frac{g_{\omega}}{\tilde{q}_{\omega}^{well}} = \frac{1}{\sum_{ij}\left[\mathbf{\Gamma}^{well} - S\frac{h}{L_{seg}}\mathbf{I}\right]_{ij}^{-1} - i\frac{C_D}{T_D}} \tag{A.28}$$

The response in an observation point could be calculated by applying eq. (A.21), in which we substitute the definition of eq. (A.20) as an influence

function for the pressure contribution at observation point r_{obs} resulting from the influx into well segment j. Furthermore we included eq. (A.25) for the distribution of flow over the segments and eq. (A.28) (with $g_\omega = m_D(\mathrm{T}_D)\tilde{q}_\omega^{well}$) for the solution of the response in the well:

$$m_{D\ obs}(\mathrm{T}_D, r_{obs}) = \frac{g_\omega(r_{obs})}{\tilde{q}_\omega^{well}} = \frac{\sum_{jl}\Gamma_j(r_{obs})\left(\mathbf{\Gamma}^{well} - S\frac{h}{L_{seg}}\mathbf{I}\right)_{jl}^{-1}}{\sum_{ij}\left(\mathbf{\Gamma}^{well} - S\frac{h}{L_{seg}}\mathbf{I}\right)_{ij}^{-1} - i\frac{C_D}{T_D}} \tag{A.29}$$

A.2 Reservoir with permeability anisotropy

For an anisotropic reservoir the horizontal and vertical permeabilities k_h and k_v are different and for the diffusivity equation we obtained:

$$\phi c\mu\frac{\partial m}{\partial t} = k_h\frac{\partial^2 m}{\partial x^2} + k_h\frac{\partial^2 m}{\partial y^2} + k_v\frac{\partial^2 m}{\partial z^2} \tag{A.30}$$

The equation could be transformed into an isotropic equation by scaling the axes. We obtained:

$$\phi c\mu\frac{\partial m}{\partial t} = k'\left[\frac{\partial^2 m}{\partial x'^2} + \frac{\partial^2 m}{\partial y'^2} + \frac{\partial^2 m}{\partial z'^2}\right] \tag{A.31}$$

$$x' = \frac{x}{\sqrt{\alpha}}; y' = \frac{y}{\sqrt{\alpha}}; z' = z\sqrt{\alpha} \tag{A.32}$$

$$\alpha = \sqrt{\frac{k_h}{k_v}};\ k' = \sqrt{k_h k_v} \tag{A.33}$$

The complete treatment of appendix A.1 applies with the notion that all the parameters that refer to length, areal or volumetric quantities must be scaled according to eqs. (A.32) and (A.33):

- the equivalent permeability reads $k^{eq} = k_h/\alpha$
- the rate q_{sc} and the wellbore storage C, being a volumetric quantity, must be scaled with $\frac{\sqrt{\alpha}}{\alpha}$
- the segments length L_{seg} must be scaled with $\frac{1}{\sqrt{\alpha}}$.
- an equivalent pay thickness $h^{eq} = h\sqrt{\alpha}$ should be considered
- an equivalent wellbore radius must be adopted (Babu and Odeh, 1989; Brigham, 1990):

$$r_w^{eq} = \frac{1+\alpha}{2\sqrt{\alpha}}r_w \tag{A.34}$$

which results from the average between the scaling factor of the horizontal direction and the scaling factor of the vertical direction.

As a consequence the dimensionless oscillation period becomes:

$$T_D^{eq} = T_D\frac{4}{(1+\alpha)^2} \tag{A.35}$$

Analogously the dimensionless wellbore storage becomes:

$$C_D^{eq} = C_D\frac{4}{(1+\alpha)^2} \tag{A.36}$$

Notice that the T_D/C_D product is not scaled. The same happens to the non-dimensionalization factor Λ (eq. (3)) because of the scaling factors applied to pay, permeability and rate vanish.

A.3 Validation

A synthetic base case was constructed. The reservoir is homogeneous and isotropic with permeability $k = 100$ mD, porosity $\phi = 0.2$, pay thickness $h = 20$ m, pressure $p_i = 130$ bar and temperature $T_R = 45$ °C. The total compressibility is $c_t = 0.00665017$ bar^{-1}. The saturating fluid composition is 90% methane gas, 5% ethane, 1% propane, 1% carbon dioxide and 3% nitrogen. The well is horizontal with a producing length of 100 m and positioned in the middle of the pay thickness; the wellbore radius is $r_w = 0.1$ m; the wellbore storage is $C = 6.41\ 10^{-6}$ m^3/Pa and the skin is S = 0. The test history is made up of 6 periods of 48 h, each alternating a rate of 500 10^3 m^3/day with a rate of 400 10^3 m^3/day every 24 h. The pressure data was analytically generated by a commercial well-test simulator, imposing a sampling rate of 10 s.

Validation against synthetic data is shown in Fig. A.1 for different skin (Fig. A.1a) and anisotropy (Fig. A.1b) scenarios. The synthetic response can deviate from the model at high frequencies (short period components), due to the imperfection of the synthetically generated spectrum. However, the agreement improves at low frequencies (long period components) and becomes good when linear flow develops. Therefore, kh and skin are correctly identified.

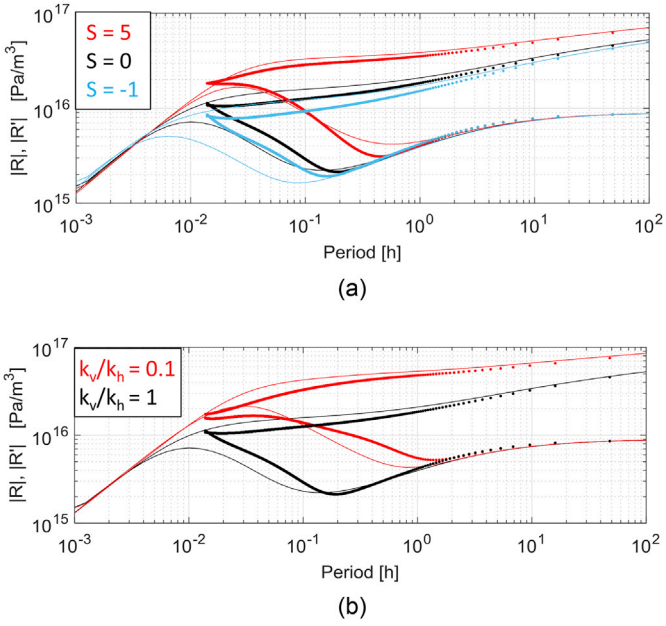

Fig. A.1. Validation of the horizontal model (solid line) against synthetic data (dotted line) in different scenarios: sensitivity to skin (b) and anisotropy (b).

A.4. Estimation of non-Darcy skin component

The analytical expression for the non-Darcy factor D derived for horizontal well geometry is (Joshi, 1991):

$$D = \frac{khM}{2\pi L^2 \mu_g R} \frac{p_{sc}}{T_{sc}} \beta \left(\frac{1}{r_w}\right) \tag{A 37}$$

where h is net pay of the formation; L is the horizontal well length, M is the gas molar mass, R is the gas constant, β is the turbulence factor, r_w is the well radius, k is the near-wellbore permeability, μ_g is gas viscosity, p_{sc} and T_{sc} stand for pressure and temperature at standard conditions, respectively. All parameters are expressed in SI units.

The turbulence factor β was calculated using the correlation suggested by Liu et al. (1995):

$$\beta = \frac{8.91 \times 10^8}{k\phi} \tau \tag{A 38}$$

where β is in 1/ft, near-wellbore permeability (k) is in mD and tortuosity (τ) was assumed as 0.67/ϕ (Pape et al., 1999).

With the parameters of the analyzed real case we obtained $D = 2.4\ 10^{-10}$ day/Sm^3. Being $450\ 10^3$ Sm^3/day the average rate value of the oscillation, the skin component due to non-Darcy effects is $1.1\ 10^{-4}$. As a consequence, the non-Darcy effects can be neglected. This result is in good agreement with the interpretation of the available FAF test.

References

Ahn, S., Horne, R., 2010. Estimating permeability distributions from pressure pulse testing. In: SPE Paper 134391, Presented at the SPE Annual Technical Conference and Exhibition, Florence, Italy, 19–22 September 2010. https://doi.org/10.2118/134391-MS.

Al-Hussainy, R., Ramey Jr., H.J., Crawford, P.B., 1966. The Flow of Real Gases through Porous Media. J. Petrol. Technol. SPE-1243-A-PA, Soc. Petrol. Eng. 18 (5), 624–636. https://doi.org/10.2118/1243-A-PA.

Amos, D.E., 1986. Algorithm 644. A portable package for Bessel functions of a complex argument and nonnegative order. ACM Trans. Math Software 12 (3), 265–273. https://doi.org/10.1145/7921.214331.

Babu, D.K., Odeh, A.S., 1989. Productivity of a horizontal well. SPE Res Eng 4 (4), 417–421. SPE-18298-PA. https://doi.org/10.2118/18298-PA.

Beretta, E., Tiani, A., Lo Presti, G., Verga, F., 2007. Value of injection testing as an alternative of conventional well testing: field experience in a sour-oil reservoir. SPE Reservoir Eval. Eng. 10 (2), 112–121. https://doi.org/10.2118/100283-PA. Paper SPE 100283-PA.

Bertolini, C., Tripaldi, G., Manassero, E., Beretta, E., Verga, F., Viberti, D., 2009. A cost effective and user friendly approach to design wireline formation tests. Am. J. Environ. Sci. 5 (6), 772–780. https://doi.org/10.3844/ajessp.2009.772.780. ISSN 1553–345X.

Black, J.H., Kipp Jr., K.L., 1981. Determination of hydrogeological parameters using sinusoidal pressure tests: a theoretical appraisal. Water Resour. Res. 17 (3), 686–692. https://doi.org/10.1029/WR017i003p00686.

Bourdet, D., 2002. Well Test Analysis: the Use of Advanced Interpretation Models. Elsevier, The Netherlands, p. 426. ISBN-10: 0444549889.

Brigham, W.E., 1990. Discussion of productivity of a horizontal well. SPE Reservoir Eng. 4 (4), 254–255 (Paper SPE 20394).

Copty, N.K., Findikakis, A.N., 2004. Stochastic analysis of pumping test drawdown data in heterogeneous geologic formations. J. Hydraul. Res. 42, 59–67. https://doi.org/10.1080/00221680409500048.

Despax, D., Dovis, R., Fedele, J.-M. and Martin, J.-P. 2004 Method and device for determining the quality of an oil well reserve. U.S. Patent 6,801,857.

Fokker, P.A., Verga, F., 2008. A Semianalytic Model for the Productivity Testing of Multiple Wells. SPE Reservoir Eval. Eng. 11 (3), 466–477. ISSN 1094–6470.

Fokker, P.A., Renner, J., Verga, F., 2013. Numerical modeling of periodic pumping tests in wells penetrating a heterogeneous aquifer. Am. J. Environ. Sci. 9 (1), 1–13. https://doi.org/10.3844/ajessp.2013.1.13.

Fokker, P.A., Salina Borello, E., Serazio, C., Verga, F., 2012. Estimating reservoir heterogeneities from pulse testing. J. Petrol. Sci. Eng. 86–87, 15–26. https://doi.org/10.1016/j.petrol.2012.03.017.

Fokker, P.A., Verga, F., 2011. Application of harmonic pulse testing to water-oil displacement. JPSE J. Petrol. Sci. Eng. 79 (3–4), 125–134. https://doi.org/10.1016/j.petrol.2011.09.004. ISSN 0920–4105.

Gringarten, A.C., 2008. From straight lines to deconvolution: The evolution of the State of the Art in well test analysis. SPE Paper 102079 SPE Reservoir Eval. Eng. 41–62. https://doi.org/10.2118/102079-PA. Feb. 2008.

Hollaender, F., Filas, J.G., Bennett, C.O., Gringarten, A.C., 2002a. Use of downhole production/reinjection for zero-emission well testing: challenges and rewards. In: Proceeding of the SPE Annual Technical Conference and Exhibition, Sept. 29-Oct. 2, SPE 77620, San Antonio, Texas. https://doi.org/10.2118/77620-MS.

Hollaender, F., Hammond, P.S., Gringarten, A.C., 2002b. Harmonic testing for continuous well and reservoir monitoring. In: Paper SPE 77692, Presented at the SPE Ann. Techn. Conf. And Exhib, San Antonio, 29 September – 2 October 2002. https://doi.org/10.2118/77692-MS.

Horne, R.N., 1994. Uncertainty in well test interpretation. In: SPE-27972-MS. University of Tulsa Centennial Petroleum Engineering Symposium, 29–31 August, Tulsa, Oklahoma. https://doi.org/10.2118/27972-MS.

Johnson, C.R., Greenkorn, R.A., Woods, E.G., 1966. Pulse testing: a new method for describing reservoir flow properties between wells. Paper SPE 1517-PA J. Pet. Technol. 1599–1604. https://doi.org/10.2118/1517-PA.

Joshi, S., 1991. Horizontal Well Technology. PennWell. ISBN10 0-87814-350-5.

Kamal, M.M., 2009. Transient well testing. In: SPE Monograph Series, vol. 23, ISBN 978-1-55563-141-3, p. 849.

Kazi-Aoual, M.N., Bonnet, G., Jouanna, P., 1991. Reconnaissance of saturated porous media by harmonic analysis. I. Direct problem. Eur. J. Mech. B/Fluids 10 (1), 51–72.

Kuo, C.H., 1972. Determination of reservoir properties from sinusoidal and multirate flow tests in one or more wells. Paper SPE 3632-PA SPE J. 12 (06), 499–507. https://doi.org/10.2118/3632-PA. Society of Petroleum Engineers.

Lee, J., Rollins, J.B., Spivey, J.P., 2003. Pressure Transient Testing. In: SPE Textbook Series, vol. 9. Society of Petroleum Engineers, ISBN 978-1-55563-099-7.

Liu, X., Civan, F., Evans, R.D., 1995. Correlation of the non-Darcy flow coefficient. J. Can. Pet. Technol. 34 (10), 50–54. PETSOC-95-10-05. https://doi.org/10.2118/95-10-05.

Morozov, P.E., 2013. Harmonic testing of hydraulically fractured wells. In: 17th European Symposium on Improved Oil Recovery. St. Petersburg, Russia, 16–18 April 2013.

Pape, H., Clauser, C., Iffland, J., 1999. Permeability prediction based on fractal pore-space geometry. Geophysics 64 (5), 1447–1460. https://doi.org/10.1190/1.1444649.

Renner, J., Messar, M., 2006. Periodic pumping tests. Geophys. J. Int. 167, 479–493. https://doi.org/10.1111/j.13365-246X.206.02984.x. Wiley-Blackwell.

Rocca, V., Viberti, D., 2013. Environmental sustainability of oil industry. Am. J. Environ. Sci. 9, 210–217. https://doi.org/10.3844/ajessp.2013.210.217. ISSN:1553–345X.

Rochon, J., Jaffrezic, V., Boutaud de La Combe, J.L., et al., 2008. Method and application of cyclic well testing with production logging. In: SPE Paper 115820, Presented at the SPE Ann. Techn. Conf, and Exhibition, Denver, 21-24 September 2008. https://doi.org/10.2118/115820-MS.

Rosa, A.J., Horne, R.N., 1997. Reservoir description by well-test analysis by use of cyclic flow-rate variation. In: Paper SPE 22698. SPE Formation Evaluation, December 1997, pp. 247–254. https://doi.org/10.2118/22698-PA, 12(4).

Salina Borello, E., Fokker, P.A., Viberti, D., Espinoza, R.V., Verga, F., 2017. Harmonic-pulse testing for non-darcy-effects identification. In: SPE Reservoir Evaluation & Engineering SPE-183649-PA. Society of Petroleum Engineers. https://doi.org/10.2118/183649-PA.

Sun, A.Y., Lu, J., Hovorka, S., 2015. A harmonic pulse testing method for leakage detection in deep subsurface storage formations. Water Resources Research. AGU. https://doi.org/10.1002/2014WR016567.

van Kruysdijk, C.P.J.W., 1988. Semianalitical modeling of pressure transients in fractured reservoir. In: SPE18169, Proceedings of the 63rd SPE Annual Technical Conference and Exhibition, Houston, Texas. https://doi.org/10.2118/18169-MS.

Verga, F., Viberti, D., Salina Borello, E., 9–12 June 2008. A new 3-D numerical model to effectively simulate injection tests. In: 70th European Association of Geoscientists and Engineers Conference and Exhibition - Incorporating SPE EUROPEC 2008. Rome, Italy. SPE-113832-MS. https://doi.org/10.2118/113832-MS.

Verga, F., Rocca, V., 2010. Green methodologies to test hydrocarbon reservoirs. Am. J. Environ. Sci. https://doi.org/10.3844/ajessp.2010.1.10. Science Publications, pp. 10, 2010, Vol. 6, pag. 1–10, ISSN: 1553–345X.

Verga, F., Viberti, D., Salina Borello, E., 2011. A new insight for reliable interpretation and design of injection tests. J. Petrol. Sci. Eng. 78 (1), 166–177. https://doi.org/10.1016/j.petrol.2011.05.002. Elsevier.

Verga, F., Viberti, D., Salina Borello, E., Serazio, C., 2015. Estimation of skin from the interpretation of injection tests in fractured reservoirs. GEAM Geoing. Ambient. Mineraria 146, 45–52. ISSN: 1121–9041.

Verga, F., Viberti, D., Serazio, C., 2012. Estimation of skin components for a partially completed damaged well from injection tests. J. Petrol. Sci. Eng. 165–174. https://doi.org/10.1016/j.petrol.2012.04.024. Elsevier, Vol., pp. 90–91.

Verga, F., Salina Borello, E., 2016. Unconventional well test technologies: a brief overview. GEAM Geoing. Ambient. Mineraria 149, 45–54. ISSN 1121–9041.

Viberti, D., 2016. Effective detrending methodology for harmonic transient pressure response. GEAM Geoing. Ambient. Mineraria 149, 55–62. ISSN 1121–9041.

Vinci, C., Steeb, H., Renner, J., 2015. The imprint of hydro-mechanics of fractures in periodic pumping tests. Geophys. J. Int. 2015 (202), 1613–1626. https://doi.org/10.1093/gji/ggv247.